Inorganic Chemistry
Cite This: Inorg. Chem. 2019, 58, 2523−2532
Article
pubs.acs.org/IC

Preliminary Assignment of Protonated and Deprotonated Homocitrates in Extracted FeMo-Cofactors by Comparisons with Molybdenum(IV) Lactates and Oxidovanadium Glycolates

Wan-Ting Jin,[†,⊥] Hongxin Wang,[‡,§,⊥] Si-Yuan Wang,[†] Christie H. Dapper,[∥] Xing Li,[†] William E. Newton,[∥] Zhao-Hui Zhou,*[,†] and Stephen P. Cramer*[,‡,§]

[†]State Key Laboratory of Physical Chemistry of Solid Surfaces, College of Chemistry and Chemical Engineering, Xiamen University, Xiamen 361005, China

[‡]Department of Chemistry, University of California, Davis, California 95616, United States

[§]Physical Biosciences Division, Lawrence Berkeley National Laboratory, Berkeley, California 94720, United States

[∥]Department of Biochemistry, Virginia Polytechnic Institute and State University, Blacksburg, Virginia 24061, United States

Supporting Information

ABSTRACT: A similar pair of protonated and deprotonated mononuclear oxidovanadium glycolates $[VO(Hglyc)(phen)(H_2O)]Cl{\cdot}2H_2O$ (**1**) and $[VO(glyc)(bpy)(H_2O)]$ (**2**) and a mixed-(de)-protonated oxidovanadium triglycolate $(NH_4)_2[VO(Hglyc)_2(glyc)]{\cdot}H_2O$ (**3**) were isolated and examined. The ≡C−O(H) (≡C−OH or ≡C−O) groups coordinated to vanadium were spectroscopically and structurally identified. The glycolate in **1** features a bidentate chelation through protonated α-hydroxy and α-carboxy groups, whereas the glycolate in **2** coordinates through deprotonated α-alkoxy and α-carboxy groups. The glycolates in **3** coordinate to vanadium through α-alkoxy or α-hydroxy and α-carboxy groups and thus have both protonated ≡C−OH and deprotonated ≡C−O bonds simultaneously. Structural investigations revealed that the longer protonated $V-O_{\alpha\text{-hydroxy}}$ bonds [2.234(2) Å and 2.244(2) Å] in **1** and **3** are close to those of FeV-cofactor (FeV-co) 2.17 Å[1] (FeMo-co 2.17 Å[2]), while deprotonated $V-O_{\alpha\text{-alkoxy}}$ bonds [**2**, 1.930(2); **3**, 1.927(2) Å] were obviously shorter. This shows a similar elongated trend as the Mo−O distances in the previously reported deprotonated vs protonated molybdenum lactates (Wang, S. Y. et al. *Dalton Trans.* **2018**, *47*, 7412−7421) and these vanadium and molybdenum complexes have the same local V/Mo-homocitrate structures as those of FeV/Mo-cos of nitrogenases. The IR spectra of these oxidovanadium and the previously synthesized molybdenum complexes including different substituted ≡C−O(H) model compounds show red-shifts for ≡C−OH vs ≡C−O alternation, which further assign the two IR bands of extracted FeMo-co at 1084 and 1031 cm^{-1} to ≡C−O and ≡C−OH vibrations, respectively. Although the structural data or IR spectra for some of the previously synthesized Mo/V complexes and extracted FeMo-co were measured earlier, this is the first time that the ≡C−O(H) coordinated peaks are assigned. The overall structural and IR results well suggest the coexistence of homocitrates coordinated with α-alkoxy (deprotonated) and α-hydroxy (protonated) groups in the extracted FeMo-co.

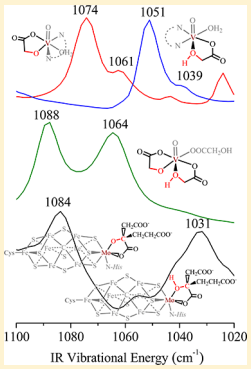

INTRODUCTION

Nitrogenases catalyze the reduction of dinitrogen (N_2) to ammonia (NH_3) in nature. The enzymes have been extensively investigated, and the structures of their catalytic active sites FeMo/V-cofactors (FeMo/V-cos) have been finally clarified as $MoFe_7S_9C$(cys)(Hhis)(*R*-homocit)[2,4−6] and VFe_7S_8C(cys)-(Hhis)(XO_3)(*R*-homocit) (H_4homocit = homocitric acid, X = C or N respectively, Hcys = cysteine, $C_3H_7NO_2S$, Hhis = histidine, $C_6H_9N_3O_2$),[1,7] where homocitrates coordinate with metal Mo or V via the oxygen atoms of α-alkoxy and α-carboxy groups and have a charge of −4.[8] Spectroscopic studies with infrared spectroscopy (IR),[9,10] magnetic circular dichroism spectroscopy (MCD),[11,12] ^{19}F nuclear magnetic resonance spectroscopy (^{19}F NMR),[13] X-ray absorption spectroscopy (XAS),[14−19] Mössbauer spectroscopy,[20,21] electron−nuclear double resonance (ENDOR),[22,23] electron spin echo envelope modulation (ESEEM),[22,23] impulsive coherent vibrational spectroscopy (ICVS),[24] nuclear resonance vibrational spectroscopy (NRVS),[25,26] and electron paramagnetic resonance (EPR)[20,27] show a low valence and paramagnetic nature for FeMo/V-cos. The charge on FeMo-cofactor (FeMo-co) has been controversial as the metal oxidation states of FeMo-co were suggested as Mo(IV)6Fe(II)1Fe(III),[28] Mo(IV)4Fe(II)-3Fe(III),[29] Mo(IV)2Fe(II)5Fe(III),[30] and Mo(III)3Fe(II)-4Fe(III), respectively.[31,32] In addition to the FeMo/V-cos' central structures, the local structure about the Mo/V-homocitrato coordination is critical for the nitrogenase studies. We have suggested a protonated model for FeMo/V-cos-based on a computational study[33] and protonated α-hydroxycarbox-

Received: November 4, 2018
Published: February 6, 2019

Downloaded via UNIV OF CALIFORNIA DAVIS on August 15, 2019 at 23:59:10 (UTC).
See https://pubs.acs.org/sharingguidelines for options on how to legitimately share published articles.

© 2019 American Chemical Society

DOI: 10.1021/acs.inorgchem.8b03108
Inorg. Chem. 2019, 58, 2523−2532

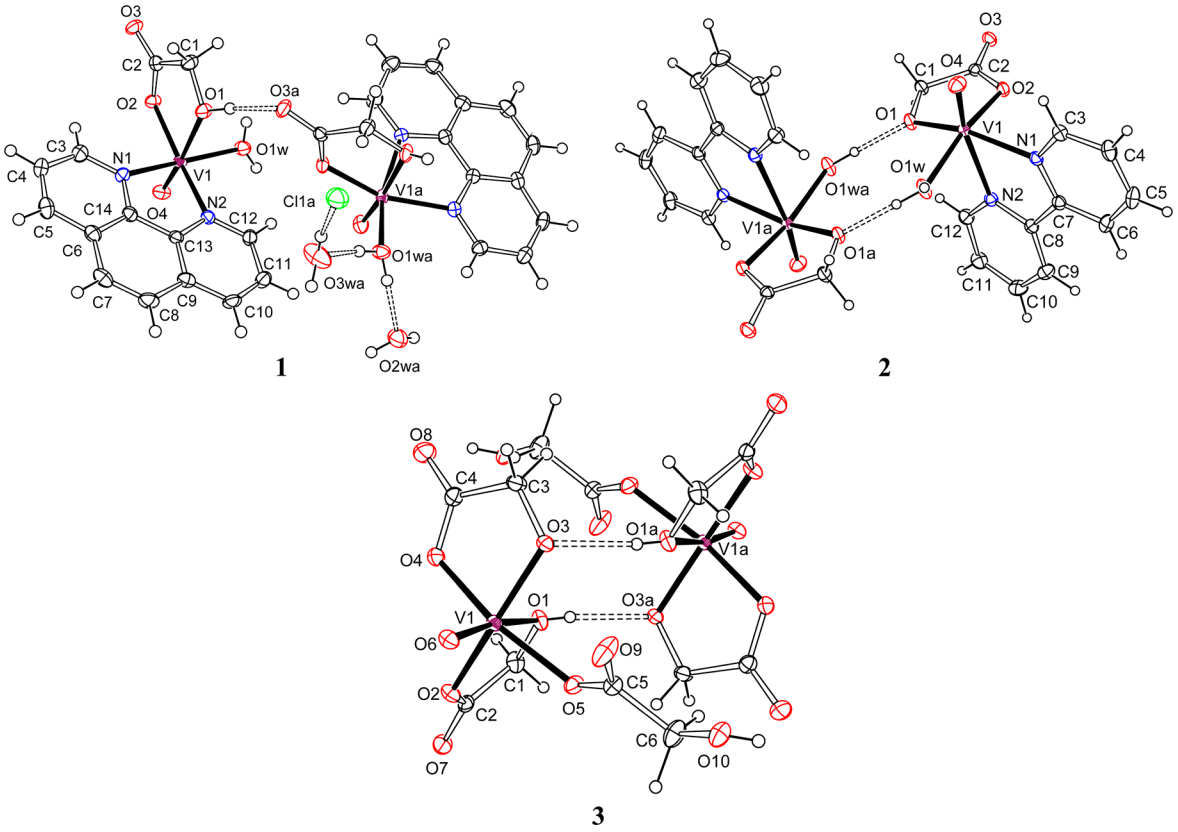

Figure 1. Environments of $[VO(Hglyc)(phen)(H_2O)]Cl{\cdot}2H_2O$ (**1**) showing hydrogen bonds between α-hydroxy groups, water molecules, and α-carboxy groups, $[VO(glyc)(bpy)(H_2O)]$ (**2**) showing hydrogen bonds between water molecules and α-alkoxy groups, and $(NH_4)_2[VO(Hglyc)_2(glyc)]{\cdot}H_2O$ (**3**) showing hydrogen bonds between α-hydroxy groups and α-alkoxy groups. Ammonium ions and lattice water molecules were omitted for clarity.

ylato oxidovanadium complexes.[34] Structural comparisons of glycolato and lactato molybdenum(IV) complexes and nitrogenases provide indirect evidence for the protonation of homocitrate in FeMo-co.[3] In addition, there are several recent theoretical computational calculations for the favorite protonation state in α-alkoxy group of homocitrate ligand of FeMo-co.[30,35−37]

Most of the previous glycolate, lactate, malate, citrate, or homocitrate bind to vanadium or molybdenum via α-alkoxy and α-carboxy and/or β-carboxy groups,[38−63] while only a small number of complexes were isolated coordinating via α-hydroxy (protonated) and α-carboxy groups.[34,64−68] As the homocitrates in the cofactors have a bidentate coordination, protonated and deprotonated molybdenum/vanadium α-hydroxycarboxylates with the similar local structures are critical for comparisons with the FeMo/V-cos and for a better clarification of their coordination environments. In this publication, we report the successfully isolated protonated and deprotonated pair of mononuclear glycolato oxidovanadium complexes: $[VO(Hglyc)(phen)(H_2O)]Cl{\cdot}2H_2O$ (**1**) and $[VO(glyc)(bpy)(H_2O)]$ (**2**) (H_2glyc = glycolic acid, bpy = 2,2′-bipyridine, phen = 1,10-phenanthroline). Oxidovanadium triglycolate $(NH_4)_2[VO(Hglyc)_2(glyc)]{\cdot}H_2O$ (**3**) with a mixed-(de)protonated state was also synthesized and analyzed. All these complexes have a similar bidentate chelated local structure as the homocitrate has in FeV-co or FeMo-co. The infrared spectrum (IR) of the extracted FeMo-co[9,69,70] has been re-examined. The structures and IR spectra of the above vanadium complexes (**1**−**3**) are compared with those of FeMo/V-cos as well as compared with the protonated and deprotonated molybdenum(IV) lactates $[Mo^{IV}_3S_4(PPh_3)_3(Hlact)_2(lact)]$,[62] $Na_2[Mo^{IV}_3SO_3(R,S\text{-lact})_3(im)_3]{\cdot}10H_2O$,[3,67] and different substituted ≡C−O(H) model compounds. Although the structural data or IR spectra for some of the previously synthesized Mo/V complexes were measured earlier, this is the first time that the ≡C−O(H) coordinated peaks are assigned. Via these comparisons, the protonated/deprotonated states of homocitrate in extracted FeMo-co are assigned experimentally and discussed systematically for the first time.

RESULTS AND DISCUSSION

Syntheses. In the preparations of **1** and **2**, the precursor V_2O_5 was reduced to VO^{2+} species by water in acidic solution under hydrothermal condition. The reactions of V_2O_5 with excess glycolic acid and N-chelated ligands are sensitive to the pH values. The deprotonated **2** was isolated at pH 3.0 in the presence of bipyridine, while the protonated **1** was obtained under low pH value of 1.0 in the presence of phenanthroline. The reactant of bipyridine or phenanthroline was not in excess. **3** was obtained from the reaction of $VOSO_4$ with 3 equiv of glycolic acid without the participation of N-chelated ligand.[24,25] The synthesis of **3** was at room temperature but the crystallization was found sensitive to the temperature and the concentration of the reactants. Moreover, the effects of pH variations between 4 and 6 and the ratio of V:ligand (1:2 or 1:3) seem less crucial for the formation of **3** in comparison

DOI: 10.1021/acs.inorgchem.8b03108
Inorg. Chem. 2019, 58, 2523−2532

with the cases in **1** and **2**. The complexes **1** and **3** are soluble in water, while **2** is insoluble.

Crystal Structures. The ORTEP diagrams of **1**−**3** are shown in the Supporting Information (SI), Figures S1−S3. The detailed X-ray crystallographic data and the selected bond distances and angles for **1**−**3** are listed as in Tables S1−S3. X-ray crystallographic analyses reveal that the glycolate in **1** coordinates bidentately to vanadium atom via protonated α-hydroxy and α-carboxy groups, while the glycolate in neutral molecule **2** coordinates via deprotonated α-alkoxy and α-carboxy groups. The V(IV) ions in **1** and **2** exist in distorted octahedral geometries with N_2O_4 donor set. In **1**, two nitrogen atoms of phenanthroline (N1 and N2) and one oxygen atom of water molecule (O1w) as well as the oxygen atom in α-carboxy group of glycolate (O2) occupy the four equatorial positions. The oxygen atom in the α-hydroxy group of glycolate (O1) is at one axial position, *trans* to the terminal oxygen atom (O4) on the other axial site. The two-dimensional (2-D) packing diagram of **1** is provided in Figure S4, showing hydrophobic π−π interaction of phenanthroline. In **2**, the oxygen atoms in α-alkoxy (O1) and α-carboxy groups (O2) are at two equatorial positions, while one coordinated water molecule (O1w) and one nitrogen atom of bpy (N1) occupy the other two equatorial positions. The other nitrogen atom of bpy (N2) is at one axial position, and the terminal oxygen atom (O4) is at the final axial site. The 2-D packing diagram of **2** is given in Figure S5, showing hydrophobic π−π interaction of bipyridine.

The vanadium ion in **3** coordinates with three glycolates, presenting a distorted octahedral geometry. One of the glycolates coordinates via α-alkoxy (O3) and α-carboxy (O4) groups, where the two oxygen atoms are at two equatorial positions. The second glycolate coordinates to vanadium via α-carboxy group (O5), leaving the α-hydroxy group (O10) free. The last glycolate coordinates via α-hydroxy (O1) and α-carboxy (O2) groups, where the α-hydroxy (O1) is *trans* to terminal oxygen atom (O6) on the final axial site. Coordinating with both of the protonated and deprotonated glycolates, **3** can serve as a mixed-(de)protonated model complex compared with **1** and **2**. The anion structure of **3** is similar to the reported potassium salt $K_2[VO(Hglyc)_2(glyc)]\cdot H_2O$.[64,65]

The structural environments near the V-glycolate coordinations of **1**−**3** are shown in Figure 1, and their hydrogen bonds are listed in Table S3. For **1**, α-hydroxy group forms a strong hydrogen bond with α-carboxy group [O1···O3a 2.71(1) Å, *a* (*x* + 1/2, −*y* + 1/2, *z* + 1/2)], and the coordinated water molecule forms strong hydrogen bonds with crystal water molecules [O1wa···O2wa 2.62(1) Å; O1wa···O3wa 2.58(1) Å]. The free chloride anions also connect with the lattice water molecules by hydrogen bonds [Cl1a···O3wa 3.03(1) Å; Cl1a···O2wb 3.05(1) Å, *b* (*x* + 1/2, −*y* + 1/2, *z* + 3/2); and Cl1a···O3wc 3.15(1) Å, *c* (*x* + 1/2, *y* − 1/2, *z* + 1)]. For **2**, the coordinated water molecules form strong hydrogen bonds with α-alkoxy and α-carboxy groups [O1w···O1a 2.58(1) Å, *a* (−*x* + 1, −*y*, −*z* + 2); O1w···O3b 2.65(1) Å, *b* (−*x* + 1, *y* − 1/2, −*z* + 3/2)]. For **3**, a mixed-(de)protonated state is formed in **3** as the strong interactions of hydrogen bonds are favorable for the proton exchange between α-alkoxy and α-hydroxy groups. The α-alkoxy O3 and α-hydroxy O1 form strong hydrogen bonds with α-hydroxy O1a and α-alkoxy O3a from the adjacent molecule, respectively. The distance of hydrogen bond [O1···O3a 2.55(1) Å, *a* (1 − *x*, 1 − *y*, 1 − *z*)] is similar to the O···O distance (2.50 Å) calculated by a protonated QM/MM model.[35]

The V−O distances of α-hydroxycarboxylato vanadium complexes vary systematically according to the bond types and the oxidation states of the vanadium ions. Theoretical bond valence calculations[71,72] (Table S4) and EPR spectra (Figure S6) gave the valence of +4 for **1**−**3**, respectively. As shown in Table 1, protonated and deprotonated oxidovanadium products **1** and **2** exhibit different V−O distances. The V1−$O1_{\alpha\text{-hydroxy}}$ distance in **1** [2.231(2) Å] (protonated) is much longer than that of V1−$O1_{\alpha\text{-alkoxy}}$ in **2** [1.931(2) Å] (deprotonated). In **3**, the V1−$O1_{\alpha\text{-hydroxy}}$ distance [2.244(2) Å] (protonated) is found longer than V1−$O3_{\alpha\text{-alkoxy}}$ distance [1.927(2) Å] (deprotonated). The difference (~0.3 Å) between V−$O_{\alpha\text{-hydroxy}}$ and V−$O_{\alpha\text{-alkoxy}}$ distances can be attributed to the *trans* effect of V=O group and the equalization of electronic cloud density resulted from the protonation. The protonation contributes about 0.1 Å to the change of V−$O_{\alpha\text{-hydroxy}}$ distance when excluding the *trans* effect from V=O group, which is supported by the protonated complexes $[VO(C_5H_9O_3)_2(C_5H_8N_2)]$[67] [V1−O2 (protonated, axial site), 2.209(2) Å; V1−O5 (protonated, equatorial site), 2.023(2) Å] and $[VO(H_2cit)(phen)]_2\cdot 6.5H_2O$ [V1−O1 (protonated, axial site), 2.203(5) Å; V2−O11 (protonated, equatorial site), 2.026(5) Å].[34] On the other hand, the *trans* effect contributing about 0.2 Å to the elongation of the V−$O_{\alpha\text{-hydroxy}}$ distance is also supported by the change of V−N distances, where the nitrogen atom on the *trans* position [2.316(2) Å] is longer than those of on the equatorial sites [$2.129(2)_{av}$ Å].

Based on the $Mo^{IV/III}$ and V^{III} proposed for FeMo-co and FeV-co,[73−76] the V/Mo−O(H) distances of α-hydroxycarboxylato vanadium/molybdenum complexes with different coordination modes and different oxidation states are listed in Table 1 for comparisons with FeV/Mo-cos. The protonated V^{IV}−$O_{\alpha\text{-hydroxy}}$ distances [$2.210(5)_{av}$ Å] are the closest distances to the corresponding V−$O_{\alpha\text{-hydroxy}/\alpha\text{-alkoxy}}$ distance in homocitrato FeV-co (2.170_{av} and 2.160_{av} Å).[1,7] While the other deprotonated V−$O_{\alpha\text{-alkoxy}}$ distances are shorter than that

Table 1. Comparisons of V/Mo−O Bond Distances (Å) in α-Hydroxycarboxylato Vanadium/Molybdenum Complexes[a]

complexes	M−O (α-hydroxy)	M−O (α-alkoxy)	M−O (α-carboxy)
1	2.231(2)		1.997(2)
2		1.931(2)	2.018(2)
3	2.244(2)	1.927(2)	$2.027(2)_{av}$
$V^{IV}O$[34,64−66]	$2.210(5)_{av}$	$1.925(4)_{av}$	$2.010(5)_{av}$
$V^{IV}{}_2O_2$[38,39,43,44]		$2.020(5)_{av}$	$2.019(6)_{av}$
$V^{IV/V}{}_2O_3$[41]		$1.856(4)_{av}$	$2.080(4)_{av}$
$V^{V}{}_2O_4$[42,44−52,65]		$1.985(8)_{av}$	$1.975(8)_{av}$
FeV-co[1] (1.35 Å)	2.170_{av}		2.112_{av}
FeV-co[7] (1.2 Å)	2.160_{av}		2.104_{av}
Mo^0 (non-nature)[68]	$2.273(8)_{av}$		$2.233(8)_{av}$
Mo^{IV}[3,67]	$2.204(4)_{av}$	$2.010(3)_{av}$	$2.121(4)_{av}$
Mo^{V}[58,59,62,63]		$2.001(8)_{av}$	$2.142(12)_{av}$
Mo^{VI}[53−61]		$1.959(8)_{av}$	$2.203(7)_{av}$
FeMo-co[2] (1.0 Å)	2.171_{av}		2.202_{av}

[a]The subscript av represents an average value. The detail data is available in Tables S5−S7 in SI.

DOI: 10.1021/acs.inorgchem.8b03108
Inorg. Chem. 2019, 58, 2523−2532

of FeV-co to different degrees, including the $V^{IV}-O_{\alpha\text{-alkoxy}}$ distance [$1.925(4)_{av}$ Å], the pentavalent $V^{V}-O_{\alpha\text{-alkoxy}}$ distance [$1.856(4)_{av}$ Å] in V_2O_3 cores as well as the $V-O_{\alpha\text{-alkoxy}}$ distances (~2.0 Å) in dimeric V_2O_2 or V_2O_4 units. The $V^{V}-O_{\alpha\text{-alkoxy}}$ distances are shorter than the $V^{IV}-O_{\alpha\text{-alkoxy}}$ distances due to the higher oxidation state of the metal center. The $V-O_{\alpha\text{-alkoxy}}$ distances in V_2O_4 or V_2O_2 units are slightly longer than the aforementioned $V^{IV}-O_{\alpha\text{-alkoxy}}$ and $V^{V}-O_{\alpha\text{-alkoxy}}$ distances due to the bridging coordination modes, where the α-alkoxy group serves as a bridging ligand. On the other hand, the distances between vanadium and α-carboxy groups (around 2.0 Å) are shorter than that of homocitrate in FeV-co (2.112_{av} and 2.104_{av} Å).[1,7]

From Table 1, the protonated $Mo-O_{\alpha\text{-hydroxy}}$ distances of α-hydroxycarboxylato molybdenum complexes are about 0.2 Å longer than those of deprotonated $Mo-O_{\alpha\text{-alkoxy}}$ bonds as described previously.[3] The $Mo^{IV}-O_{\alpha\text{-hydroxy}}$ distances of 2.179(4) Å and 2.228(4) Å in $[Mo^{IV}{}_3S_4(PPh_3)_3(Hlact)_2lact]$[67] are close to the value of 2.17_{av} Å in FeMo-co,[2] while the $Mo^{IV}-O_{\alpha\text{-alkoxy}}$ distances of $2.022(3)_{av}$ Å in $Na_2[Mo_3SO_3(lact)_3(im)_3]\cdot 10H_2O$[3] are obviously shorter. This is also true for the $Mo^{0}-O_{\alpha\text{-hydroxy}}$ (non-nature) bonds, which are the longest protonated distances due to their lowest oxidation states. In comparison with the bond distances of these similar compounds, the vanadium/molybdenum atoms in cofactors might have weak interactions with homocitrates and protonated α-hydroxy coordinations (Figure 2).

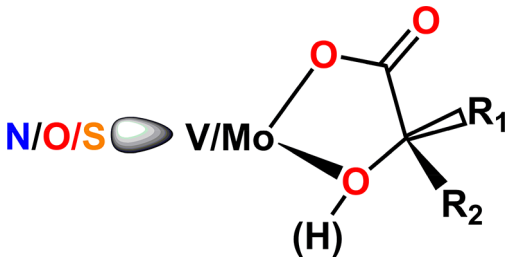

Figure 2. Structures of model vanadium/molybdenum hydroxycarboxylates with low oxidation states.

^{13}C NMR Measurement. Solution ^{13}C NMR spectrum shown in Figure 3 provides valuable information on the coordination environment and chemical behavior of **1**. The resonances for α-carboxy (α-CO_2) and α-hydroxy (α-COH) groups in **1** are at 178.9 and 61.9 ppm, respectively, showing downfield shifts compared with free glycolic acid (α-CO_2 177.0 ppm; α-COH 60.2 ppm). The small shifts indicated that the protonated coordination environment of glycolate ligand in **1** was close to the free state, which implies a weak coordination between oxidovanadium ion and α-hydroxy group.

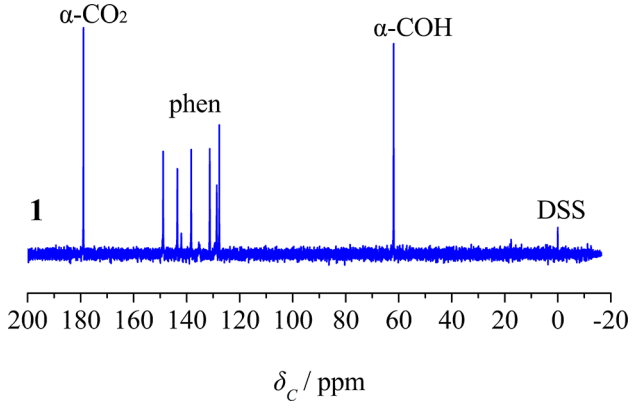

Figure 3. Solution ^{13}C NMR spectrum of $[VO(Hglyc)(phen)(H_2O)]Cl\cdot 2H_2O$ (**1**) in D_2O.

FT-IR Measurements. The FT-infrared spectra of the solids **1** and **2** in the regions of 1800–400 cm^{-1} are shown in Figure 4, and the spectrum for **3** is shown in Figure S7. To

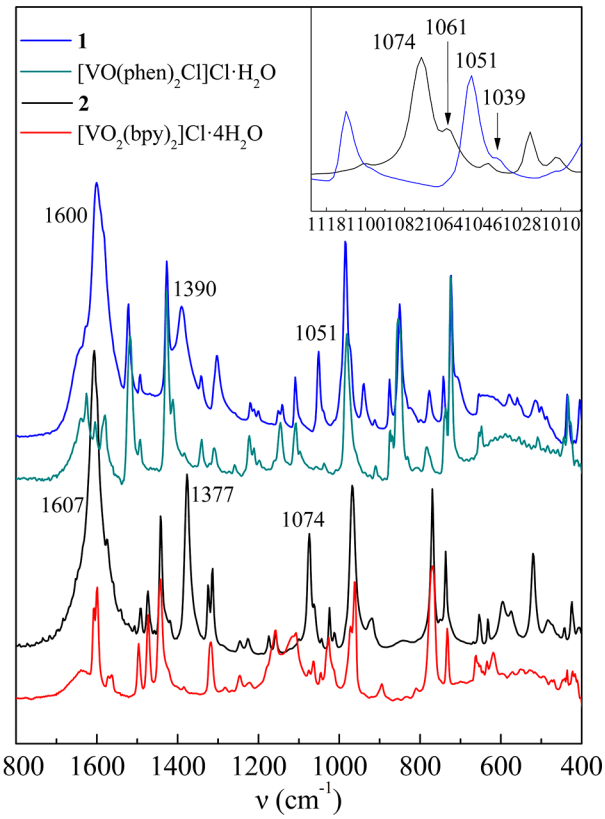

Figure 4. FT-IR spectra of $[VO(Hglyc)(phen)(H_2O)]Cl\cdot 2H_2O$ (**1**), $[VO(phen)_2Cl]Cl\cdot H_2O$, $[VO(glyc)(bpy)(H_2O)]$ (**2**), and $[VO_2(bpy)_2]Cl\cdot 4H_2O$ in the regions of 1800–400 cm^{-1}.

eliminate the interference peaks from bipyridine and phenanthroline, the IR spectra of previously reported complexes $[VO(phen)_2Cl]Cl\cdot H_2O$[77] and $[VO_2(bpy)_2]Cl\cdot 4H_2O$[78] were also re-recorded (Figure 4). The spectra of **1**–**3** show well-resolved strong and sharp absorption bands for the carboxy groups of coordinated glycolates. For **1** and **2**, the asymmetric stretching vibrations $\nu_{as}(CO_2^-)$ are observed at 1600 and 1607 cm^{-1}, and the corresponding symmetric stretching vibrations $\nu_s(CO_2^-)$ appear at 1390 and 1377 cm^{-1}, respectively. For **3**, the asymmetric stretching vibrations $\nu_{as}(CO_2^-)$ are observed at 1655, 1649, 1630, 1597, 1561, and 1554 cm^{-1}. The corresponding symmetric stretches $\nu_s(CO_2^-)$ appear at 1421, 1412, 1356, and 1317 cm^{-1}. All of the carboxy absorptions shift to lower frequencies in comparison with those of free ligand H_2glyc. The frequency differences $\Delta[\nu_{as}(CO_2^-) - \nu_s(CO_2^-)]$[79] are greater than 200 cm^{-1}, which are consistent with the monodentate fashion that the carboxy group is coordinated to the metal ion, and are in agreement with the structural data observed with X-ray crystallography. The vibrational bands above 2000 cm^{-1} are assigned to C–H, N–H, and O–H stretching modes. The

DOI: 10.1021/acs.inorgchem.8b03108
Inorg. Chem. 2019, 58, 2523–2532

features in the region of 920−990 cm^{-1} indicate the existence of a V=O bond and are consistent with the values observed in other vanadium complexes.[38,41,43,80,81]

The C−O stretching vibrations in alcohols produce bands in the region 1260−1000 cm^{-1}.[82] Based on the observations on some alcohols and α-hydroxycarboxylic acids listed in Table S7, the peaks of **1** at 1051.3 and 1039.5 cm^{-1} are assigned to the protonated C−OH stretching vibrations, while the peaks of **2** at higher frequencies 1074.4 and 1061.0 cm^{-1} are assigned to the deprotonated C−O stretching vibrations.[65] All of the C−O(H) absorptions were shifted to lower frequencies in comparison with H_2glyc at 1086 cm^{-1}. The comparison of the IR spectra for **1**, **2**, $[VO(phen)_2Cl]Cl{\cdot}H_2O$,[77] and $[VO_2(bpy)_2]Cl{\cdot}4H_2O$[78] also supports the assignments for the peaks in Figure 4. The protonated glycolato oxidovanadium complex **1** shows a red-shift (about 23 cm^{-1}) in comparison with the deprotonated glycolato oxidovanadium complex **2**. Besides, theoretical frequency calculations using Gaussian 09 for **1** and **2** (Figure S8) also exhibit the same red-shift trend, which show ν(C−O) and ν(C−OH) at 1098 and 1036 cm^{-1}, respectively. This is the first time a similar pair of protonated and deprotonated complexes with the same V-homocitrate local coordination structure was investigated.

In Figure S7, the C−O stretching vibrations of **3** are more complex due to the multiple types of coordination of glycolates. Complex **3** containing both α-alkoxy and α-hydroxy groups exhibits two absorptions at 1088.3 and 1064.5 cm^{-1}, which are preliminarily assigned to the deprotonated C−$O_{α\text{-alkoxy}}$ and protonated C−$O_{α\text{-hydroxy}}$ stretching vibrations, respectively. Therefore, complex **3** can serve as a mixed-(de)protonated model compound for the coexisting state of protonated and deprotonated homocitrates in nitrogenase.

Table 2 shows characteristic peaks of C−O or C−OH stretching vibrations of α-hydroxycarboxylato vanadium and molybdenum complexes, which serve as model compounds for FeV-co and FeMo-co. In analyzing these C−O/C−OH stretching vibrations, we have found that, whether in vanadium or molybdenum complexes, the protonated C−OH stretching vibrational frequencies are generally lower than the deprotonated C−O stretching vibrations. For example, previously reported lactato molybdenum(IV) complexes $Na_2[Mo_3SO_3(lact)_3(im)_3]{\cdot}10H_2O$[3] with α-alkoxy coordination and $[Mo^{IV}{}_3S_4(PPh_3)_3(Hlact)_2lact]$[67] with α-alkoxy/α-hydroxy coordinations also show red-shifts from 1095.4, 1060.8, 1049.9 to 1090, 1036 cm^{-1}, respectively. In brief, the ν(C−OH) of these complexes can be as low as 1030 cm^{-1}, or even shifted to 1005 cm^{-1}, while ν(C−O) are almost around 1080 cm^{-1}. This is because the protonation weakens the strength of the C−O bond, resulting in the red-shift of vibrational frequency. As we can see in Table 2, the C−$O_{α\text{-hydroxy}}$ distances (1.44_{av} Å) of protonated compounds are subtly longer than C−$O_{α\text{-alkoxy}}$ distances of deprotonated compounds (1.415_{av} Å) and comparable with those of FeV-co (1.443_{av} Å) and FeMo-co (1.449_{av} Å). This is in accordance with the proposition of α-hydroxy coordination models in cofactors. The C−$O_{α\text{-alkoxy}}$ vibrational frequencies of deprotonated homocitrate model complexes, $[V_2O_3(phen)_3(R,S\text{-}H_2homocit)_2(H_2O)]Cl{\cdot}6H_2O$[41] and $K_2[Mo^{VI}O_2(R,S\text{-}H_2homocit)_2]{\cdot}2H_2O$,[61] were both observed to have an IR peak at 1084 cm^{-1}. Although model complexes of protonated Mo/V homocitrates have not yet been obtained, the corresponding IR absorptions of the C−$O_{α\text{-hydroxy}}$ bonds should shift to lower wave numbers according to the Hook law.

Table 2. C−O(H) Bond Distances (Å) and IR Vibrational Frequencies (cm^{-1}) of C−$O_{α\text{-alkoxy}}$ or C−$O_{α\text{-hydroxy}}$ Groups

samples	C−O(H) distances (Å)	frequencies (cm^{-1})
Protonated		
$[V^{IV}O(Hglyc)(phen)(H_2O)]Cl{\cdot}2H_2O$ (**1**)	1.422(4)	1051.4m, 1039.5w
$[V^{IV}O(Hmal)(bpy)]{\cdot}H_2O$[34]	1.433(4)	1085.3m, 1030.5m
$[V^{IV}O(S\text{-}Hcitmal)(bpy)]{\cdot}2H_2O$[34]	1.444(5)	1059.6w, 1035.5m
$[V^{IV}O(H_2cit)(bpy)]{\cdot}2H_2O$[34]	1.440(8)	1068.7m, 1032.7s
$(Et_4N)_2[Mo^0(Hmal)(CO)_3]$[68] (non-nature)	1.440(5)	1007w
$(Et_4N)_3[Mo^0(Hcit)(CO)_3]$[68] (non-nature)	1.462(4)	1005m
$(Et_4N)_2[Mo^0(Hcitmal)(CO)_3]$[68] (non-nature)	1.44(1)	1007w
Deprotonated		
$[V^{IV}O(glyc)(bpy)(H_2O)]$ (**2**)	1.412(3)	1074.4s, 1061.0m
$K_2[Mo^{VI}O_2(glyc)_2]{\cdot}H_2O$[53]	$1.404(5)_{av}$	1094s, 1082s, 1066s
$[Mo_3SO_3(glyc)_2(im)_5]{\cdot}im{\cdot}H_2O$[3]	$1.408(3)_{av}$	1099.0m, 1070.9s
$\{Na_2[Mo^{VI}O_2(S\text{-}lact)_2]\}_3{\cdot}13H_2O$[53]	1.427(8)	1085s, 1057s
$Na_2[Mo_3SO_3(R,S\text{-}lact)_3(im)_3]{\cdot}10H_2O$[3]	$1.404(4)_{av}$	1095.4m, 1060.8m, 1049.9m
$[V^{IV/V}{}_2O_3(phen)_3(Hcit)_2(phen)_3O_3V_2]{\cdot}12H_2O$[41]	1.410(2)	1073m
$(NH_4)_4[(Mo^{VI}O_3(cit)]{\cdot}2H_2O$[57]	1.422(3)	1093m, 1073m
$[(Mo^{V}O)_2O(bpy)_2(H_2cit)_2]{\cdot}4H_2O$[58]	$1.435(5)_{av}$	1078m
$[(Mo^{V}O_2)_2(phen)(H_2cit)(H_2O)_2]{\cdot}H_2O$[58]	1.419(8)	1086m
$[V^{IV/V}{}_2O_3(phen)_3$ (R,S-$H_2homocit)_2(H_2O)]Cl{\cdot}6H_2O$[41]	1.410(7)	1084m
$K_2[Mo^{VI}O_2(R,S\text{-}H_2homocit)_2]{\cdot}2H_2O$[61]	$1.419(2)_{av}$	1083.8m
Protonated and Deprotonated		
$(NH_4)_2[V^{IV}O(Hglyc)_2(glyc)]{\cdot}H_2O$ (**3**)	$1.415(4)_{av}$	1088.3s, 1064.5s
$[Mo^{IV}{}_3S_4(PPh_3)_3(Hlact)_2lact]$[67]	$1.431(9)_{av}$	1090s, 1036s
FeV-co	1.443_{av}[1,7]	–
FeMo-co	1.449_{av}[3]	1084s, 1031s

Re-Evaluation of IR Spectrum of Extracted FeMo-co.

To identify the protonation state of homocitrate in FeMo-co, we have re-examined the IR spectrum of FeMo-co extracted from nitrogenase purified from *Azotobacter vinelandii* (Figure 5). The IR spectrum for the film sample of extracted FeMo-co exhibits absorption peaks at 1672, 1606, 1483, 1457, 1399, 1375, 1332, 1319, 1242, 1183, 1084, 1031, 1006, 984, 801, 748, 698, 647, 614, and 578 cm^{-1}, respectively. Qualitative assignments of extracted FeMo-co are given in Table 3, where the vibrations of the following groups COO^-, C−C, C−O, Mo−O, tetraethylammonium chloride (TEAC), and *N*-methylformamide (NMF) are identified. The IR spectrum for TEAC is also shown in Figure 5.

The complexes' C−O(H) stretching frequencies in Table 2 can serve as references for the C−O(H) vibrations in FeMo-co. The oxidation state of Mo atom in FeMo-co was assigned as Mo(IV)[74] and Mo(III)[75,76] previously, which are close to those of Mo(IV) complexes, such as $Na_2[Mo^{IV}{}_3SO_3(R,S\text{-}lact)_3(im)_3]{\cdot}10H_2O$[3] and $[Mo^{IV}{}_3S_4(PPh_3)_3(Hlact)_2lact]$.[67] Therefore, the C−OH or C−O vibrational frequency of FeMo-co is inferred to be around 1030 or 1080 cm^{-1},

DOI: 10.1021/acs.inorgchem.8b03108
Inorg. Chem. 2019, 58, 2523−2532

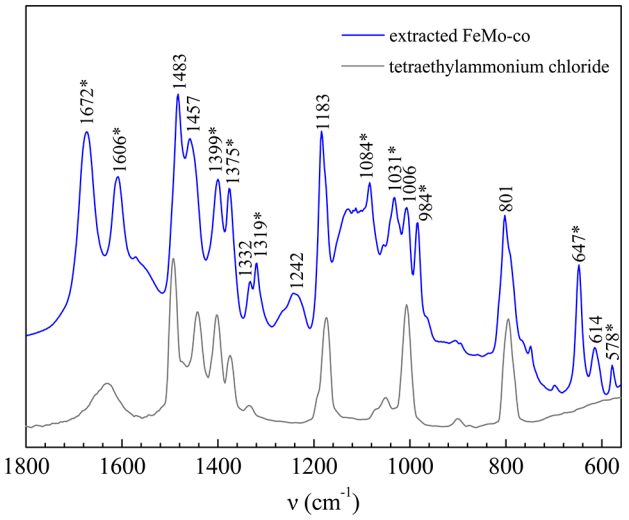

Figure 5. FT-IR spectra of extracted FeMo-co and tetraethylammonium chloride (TEAC) in the region of 1800−560 cm^{-1}.

Table 3. Qualitative Assignments of the Most Intensive Bands in IR Spectrum of Extracted FeMo-co

frequency assignments (cm^{-1})			
	our work	Orme-Johnson's work[9]	
1672	$\nu_{as}(CO_2^-)$ + partial NMF	1664	NMF
1606	$\nu_{as}(CO_2^-)$	1600	$\nu_{as}(CO_2)$
1483	TEAC		
1457	TEAC		
1399	$\nu_s(CO_2^-)$ + partial TEAC	1389	$\nu_s(CO_2^-)$
1375		1357	$\nu_s(CO_2^-)$
1332	TEAC		
1319	–		
1242	NMF		
1183	ν(C−C) + partial TEAC	1127	dithionite
1084	ν(C−O)		
1031	ν(C−OH)		
1006	TEAC	1002	
984	–		
801	TEAC	842	
647	–		
614	NMF		
578	ν(Mo−O)		

respectively, which are analogous to the assignments of C−OH or C−O vibrations in complexes **1** and **2**.

The peak at 1672 cm^{-1} in extracted FeMo-co IR is assigned to the asymmetric vibration $\nu_{as}(CO_2^-)$ of homocitrate, in comparison with 1675 cm^{-1} for $K_2[Mo^{VI}O_2(R,S\text{-}H_2homocit)_2]\cdot 2H_2O$.[61] It was assigned only to NMF in the previous reference.[9] We therefore assign this peak to $\nu_{as}(CO_2^-)$ of extracted FeMo-co and the NMF absorptions.

The peak at 1606 cm^{-1} is assigned to the asymmetric vibration $\nu_{as}(CO_2^-)$ for homocitrate in extracted FeMo-co, corresponding to 1589 cm^{-1} for $K_2[Mo^{VI}O_2(R,S\text{-}H_2homocit)_2]\cdot 2H_2O$[61] and 1607 cm^{-1} for $[V_2O_3(phen)_3(R,S\text{-}H_2homocit)_2(H_2O)]Cl\cdot 6H_2O$.[41] This is consistent with the previous assignment by Orme-Johnson and co-workers,[9] but with a clearer resolution.

The peaks at 1399 and 1375 cm^{-1} for extracted FeMo-co should belong to the symmetric carboxyl vibrations, in comparison with the peaks 1390 cm^{-1} for $K_2[Mo^{VI}O_2(R,S\text{-}H_2homocit)_2]\cdot 2H_2O$[61] and 1383 and 1346 cm^{-1} for $[V_2O_3(phen)_3(R,S\text{-}H_2homocit)_2(H_2O)]Cl\cdot 6H_2O$,[41] which are consistent with Orme-Johnson's observation.[9] But the peaks in the range of 1493−1375 cm^{-1} also overlap with strong absorptions of TEAC, therefore 1399 and 1375 cm^{-1} could be assigned to $\nu_s(CO_2^-)$ of extracted FeMo-co and the TEAC absorptions.

The peak at 1183 cm^{-1} for extracted FeMo-co is assigned to the C−C vibration, while the 578 cm^{-1} peak in the FeMo-co spectrum is assigned to Mo−O vibration in comparison with 553 and 540 cm^{-1} in $K_2[Mo^{VI}O_2(R,S\text{-}H_2homocit)_2]\cdot 2H_2O$.[61] The strong peaks at 1006 and 801 cm^{-1} are assigned to the vibrations of TEAC.

Most importantly, the peaks at 1083 and 1031 cm^{-1} in the IR-spectrum of extracted FeMo-co are assigned to C−O and C−OH vibrations as mentioned in the beginning of this section. The absorption at 1031 cm^{-1} is corresponding to the protonated C−OH at 1051 and 1039 cm^{-1} in **1**, 1032 cm^{-1} in $[V^{IV}O(H_2cit)(bpy)]\cdot 2H_2O$,[34] and 1036 cm^{-1} in $[Mo^{IV}{}_3S_4(PPh_3)_3(Hlact)_2(lact)]$,[62] respectively. The peak at 1083 cm^{-1} is corresponding to the deprotonated model compounds $[V^{IV/V}{}_2O_3(phen)_3(R,S\text{-}H_2homocit)_2(H_2O)]Cl\cdot 6H_2O$[41] (1084 cm^{-1}) and $K_2[Mo^{VI}O_2(R,S\text{-}H_2homocit)_2]\cdot 2H_2O$[61] (1084 cm^{-1}). Therefore, protonated and deprotonated homocitrates coexist in the particular extracted FeMo-co film evaluated here.

CONCLUSIONS

Here, a pair of mononuclear protonated and deprotonated glycolato oxidovanadium complexes with similar bidentate chelated local structure of V-homocitrate: $[VO(Hglyc)(phen)(H_2O)]Cl\cdot 2H_2O$ (**1**) and $[VO(glyc)(bpy)(H_2O)]$ (**2**) are reported. The glycolate ligand coordinated bidentately to the central vanadium with protonated α-hydroxy and α-carboxy oxygen atoms in **1**, while coordinated with deprotonated α-alkoxy and α-carboxy oxygen atoms in **2**. In oxidovanadium triglycolate $(NH_4)_2[VO(Hglyc)_2(glyc)]\cdot H_2O$ (**3**), the glycolate ligands coordinated to vanadium through protonated α-hydroxy, deprotonated α-alkoxy, and α-carboxy groups. The crystal structural data show that the elongated protonated V/Mo−$O_{\alpha\text{-hydroxy}}$ distances are close to those of FeV/Mo-cos, which indicate a proposed protonated α-hydroxy group in FeV/Mo-cos.

Based on the comparisons of C−$O_{\alpha\text{-alkoxy}/\alpha\text{-hydroxy}}$ stretching vibrations of vanadium and molybdenum complexes, the C−OH stretching vibration will shift to a lower wavenumber in comparison with C−O stretching vibrations. The IR spectrum for extracted FeMo-co shows two absorption peaks at 1084 and 1031 cm^{-1}, indicating a coexistence of deprotonated α-alkoxy and protonated α-hydroxy coordination in the Mo-homocitrate of FeMo-co. The IR spectra for some of the previously reported Mo/V complexes were also cited to compare with the three special oxidovanadium complexes in this publication and with the extracted FeMo-co. Nevertheless, the ≡C−O(H) peaks are assigned for the first time for all these samples.

EXPERIMENTAL SECTION

Materials and Instrumentation. All solvents and reagents (in commercially analytical grade) were used without further purification. The pH value was determined by a PHB-8 digital pH meter. Elemental analyses (for C, H and N) were performed with a Vario EL III CHN elemental analyzer. Infrared spectra were measured in the

DOI: 10.1021/acs.inorgchem.8b03108
Inorg. Chem. 2019, 58, 2523−2532

range 400−4000 cm^{-1} on a Nicolet FT-IR spectrometer with samples in KBr plates. The solid diffused UV−vis spectra were recorded at 293 K using a Cary 5000 UV−vis-NIR spectrophotometer in the 200−800 nm range. Solid and solution (in DMSO) electron paramagnetic resonance (EPR) spectra were obtained by a Bruker EMX-10/12 spectrometer using crystalline samples at low temperatures. The FTIR of extracted FeMo-co was measured using Bruker V66/S and V70/v FTIR spectrometers at UCD and LBNL, with FeMo-co film on ZnSe or polyethylene plates, respectively, for different wavenumber regions. To minimize the NMF amount left in the FeMo-co film, the samples were pumped for more than 8 h before the measurement. Solution ^{13}C NMR spectrum of **1** with long time superimposition was recorded on a Bruker Avance III 600 MHz NMR spectrometer with D_2O, using sodium 2,2-dimethyl-2-silapentane-5-sulfonate (DSS) as an internal reference.

Cell Growth and Purification of Nitrogenase Proteins. The *Aν* wild-type strain was grown in the absence of a fixed-nitrogen source in a 24-L fermenter at 30 °C in a modified, liquid Burk medium.[83] All cultures contained 20 μM $FeCl_3$ and 10 μM Na_2MoO_4 and were grown to a final cell density of 250 Klett units recorded on a Klett−Summerson meter equipped with a number 54 filter. All manipulations of nitrogenase proteins were performed anaerobically using either a Schlenk line or an anaerobic glovebox operating at less than 1 ppm of O_2. After harvesting, cell extracts were prepared by diluting the whole cells with an equal amount of 50 mM Tris pH 8.0 buffer prior to passing through a French pressure cell and a centrifuge at 98000*g* for 90 min. Nitrogenase component proteins were separated by anaerobic Q-Sepharose anion exchange column chromatography using a linear NaCl concentration gradient. *Aν*2 was purified to homogeneity by fractionation from a second Q-Sepharose column. *Aν*1 was further purified by Sephacryl S-200 gel filtration and phenyl-Sepharose hydrophobic-interaction chromatography.[84] The purified nitrogenase proteins were concentrated individually using an Amicon microfiltration pressure concentrator before buffer exchange to 25 mM HEPES pH 7.5, 100 mM NaCl, 10 mM $MgCl_2$, and 2 mM $Na_2S_2O_4$ by dialysis at 4 °C. Purified wild-type *Aν*1 had specific activities of 2200 nmol of H_2 $(min{\cdot}mg{\cdot}protein)^{-1}$ at 30 °C, when assayed in the presence of an optimal amount of the purified complementary component protein as described previously.[84] Protein concentrations were determined by the Lowry method.

Extraction of FeMo-co from *Aν*1. *Aν*1 was purified as above through the gel-filtration step, yielding protein with a specific activity of ∼1000 nmol of H_2 $(min{\cdot}mg\ protein)^{-1}$ and a Mo content of ∼1 g·atom per mol of *Aν*1. After dialysis to lower the NaCl concentration, the *Aν*1 was loaded onto a DE-52 cellulose column that had been washed with 50 mM Tris pH 7.4 buffer containing 2 mM $Na_2S_2O_4$. The bound protein was washed with *N*,*N*-dimethylformamide containing 50 mM 2,2′- bipyridine, 5 mM phosphate buffer pH 8, with 2 mM $Na_2S_2O_4$, and water (ca. 5% v/v) until the non-cofactor iron was completely eluted. The column was then washed with *N*-methylformamide (NMF) containing 5 mM phosphate buffer pH 8, with 2 mM $Na_2S_2O_4$, and water (ca. 5% v/v), and FeMoco was then eluted with NMF that contained 500 mM tetraethylammonium chloride, 5 mM phosphate buffer pH 8, with 2 mM $Na_2S_2O_4$, and water (ca. 5% v/v). The eluted FeMo-co was concentrated approximately 20-fold by distilling off the NMF under vacuum at 40 °C. FeMo-co was assayed[85] by reconstitution of the DJ42 *Aν* strain, which has a deletion for the FeMo-co biosynthetic genes *nif*ENX. The FeMo-co used in this study activated a DJ42 crude extract and produced 75 nmol of H_2 $(min{\cdot}mg\ protein)^{-1}$.

X-ray Crystallography. The crystal structural data for **1**−**3** were collected on an Oxford Gemini CCD diffractometer, with graphite monochromatic Mo−Kα radiation (λ = 0.71073 Å) at 173 K. Mutiscan absorption corrections were applied. Direct methods structure solution, difference Fourier calculations, and full-matrix least-squares refinements against F^2 were performed with SHELXL-2018/3 using the OLEX2 crystallographic software package.[86−88] All non-hydrogen atoms were refined anisotropically, while the hydrogen atoms of carbon atoms were generated geometrically and the hydrogen atoms of water molecules, ammonium ions, and hydroxyl groups were located from differential Fourier maps and refined isotropically. To obtain reasonable structures, some "dfix" restraints were applied to the water molecules and hydroxyl group. The distances of O−H were restrained to be 0.85 Å: O1w−H1wA, O1w−H1wB, O2w−H1wA, O2w−H1wB, O3w−H1wA, O3w−H1wB, and O1−H1 in **1**, and O1w−H1wA and O1w−H1wB in **2**. The angles of H−O−H were restrained by fixing the distances of the two hydrogen atoms at 1.39 Å: H1wA···H1wB, H2wA···H2 Wb, and H3wA···H3wB in **1**.

Computational Method. The geometry optimizations and frequency calculations were carried out using Gaussian 09.[89] The molecular structures of $[VO(Hglyc)(phen)(H_2O)]^+$ cation of **1** and neutral molecule of **2** were optimized separately using density functional theory method. The 6-31G* (d, p) basis set was used for all atoms, and B3LYP exchange−correlation functional was utilized to evaluate their performances in reproducing the solid-state structures and spectroscopic properties.

*Synthesis of [VO(Hglyc)(phen)(H$_2$O)]Cl·2H$_2$O (**1**).* Vanadium pentoxide V_2O_5 (0.091 g, 0.50 mmol), glycolic acid in excess (0.60 g, 8.0 mmol), and 1,10-phenanthroline (0.10 g, 0.51 mmol) were dissolved in water (8 mL) with continuous stirring. The pH value was adjusted to 1.0 with dilute hydrochloric acid (1.0 M). The mixture was placed in a Teflon-lined stainless steel bomb. The bomb was heated to 443 K for 3 days and cooled with programmed control. The bluish green solution was evaporated at room temperature for 2 months to grow blue crystals. The crystals were collected and washed with ethanol to afford **1** (0.067 g, 32% yield based on phen). Elemental analysis (calcd for $C_{14}H_{11}ClN_2O_7V$): C, 40.8; H, 4.2; N, 6.8%. Found: C, 40.6; H, 4.0; N, 6.4%. IR (cm^{-1}): 3435(s), 3367(s), 3230(s), 3096(s), 3061(s), 2665(s), 2595(s), 2135(m), 2002(w), 1966(w), 1934(w), 1600(vs), 1522(s), 1493(m), 1426(s), 1390(s), 1341(m), 1303(m), 1220(w), 1211(w), 1200(w), 1151(w), 1141(w), 1109(m), 1051(m), 1041(w), 985(s), 940(m), 912(w), 875(m), 850(m), 799(w), 777(m), 742(m), 723(s), 654(m), 579(m), 559(m), 515(m), 500(m), 487(m), 435(m).

*Synthesis of [VO(glyc)(bpy)(H$_2$O)] (**2**).* Vanadium pentoxide V_2O_5 (0.091 g, 0.50 mmol), glycolic acid in excess (0.40 g, 5.26 mmol), and 2,2′-bipyridine (0.080 g, 0.50 mmol) were dissolved in water (8.0 mL) with continuous stirring. The pH value was adjusted to 3.0 with dilute potassium hydroxide (1.0 M). The bomb was heated to 443 K for 3 days and cooled with programmed control. The brown green crystals were collected and washed with ethanol to afford **2** (0.090 g, 56% yield based on bpy). Elemental analysis (calcd for $C_{12}H_{12}N_2O_5V$): C, 45.7; H, 3.8; N, 8.9%. Found: C, 45.4; H, 3.6; N, 8.5%. IR (cm^{-1}): 3435(m), 3111(m), 3100(m), 3057(m), 3033(m), 2863(m), 2829(m), 1607(vs), 1575(m), 1492(m), 1474(m), 1442(s), 1377(s), 1324(m), 1314(m), 1246(w), 1226(w), 1174(w), 1157(w), 1100(w), 1074(s), 1061(m), 1044(w), 1024(m), 1012(w), 968(s), 919(m), 769(s), 736(s), 653(m), 632(m), 596(m), 575(m), 520(m), 483(w), 443(w), 425(w).

*Synthesis of (NH$_4$)$_2$[VO(Hglyc)$_2$(glyc)]·H$_2$O (**3**).*[24,25] Oxidovanadium sulfate (326 mg, 2.0 mmol) and glycolic acid (456 mg, 6.0 mmol) were dissolved in water (5.0 mL). The pH value of the solution was adjusted to 5.0 by concentrated ammonium hydroxide with continuous stirring. After 1 month, the light purple precipitate was collected and washed with water and ethanol to afford **3**. (0.174g, 25% yield based on vanadium). Anal. calcd for $C_6H_{18}N_2O_{11}V$: C, 20.9; H, 5.3; N, 8.1. Found: C, 20.8; H, 5.5; N, 8.0 (%). IR (cm^{-1}): 3399(m), 3180(s), 3053(s), 2914(m), 2840(m), 1655(s), 1649(s), 1630(s), 1597(m), 1561(s), 1554(s), 1502(w), 1465(m), 1449(m), 1421(s), 1412(s), 1356(s), 1317(s), 1247(w), 1237(w), 1088(s), 1065(s), 1006(w), 955(s), 935(s), 740(m), 716(m), 603(m), 583(m), 568(m), 522(s), 483(w), 477(w), 444(m), 432(m), 419(m).

■ ASSOCIATED CONTENT

Supporting Information

The Supporting Information is available free of charge on the ACS Publications website at DOI: 10.1021/acs.inorgchem.8b03108.

DOI: 10.1021/acs.inorgchem.8b03108
Inorg. Chem. 2019, 58, 2523−2532

Three parts of information: Part I: Syntheses of $[VO(phen)_2Cl]Cl{\cdot}H_2O$[77] and $[VO_2(bpy)_2]Cl{\cdot}4H_2O$,[78] ORTEP plots, packing diagrams, UV−vis, FT-IR, EPR, crystallographic data, selected bond distances and angles, hydrogen bonds, valence bond analyses for complexes **1**−**3**. The comparisons of V/Mo−O distances in α-hydroxycarboxylato vanadium/molybdenum complexes. Part II: FT-IR spectrum of extracted FeMo-co. Part III: IR spectra of all the compounds in Tables 2 and 3 (PDF)

Accession Codes

CCDC 1472398−1472399 and 1570694 contain the supplementary crystallographic data for this paper. These data can be obtained free of charge via www.ccdc.cam.ac.uk/data_request/cif, or by emailing data_request@ccdc.cam.ac.uk, or by contacting The Cambridge Crystallographic Data Centre, 12 Union Road, Cambridge CB2 1EZ, UK; fax: +44 1223 336033.

AUTHOR INFORMATION

Corresponding Authors

*Zhao-Hui Zhou. E-mail: zhzhou@xmu.edu.cn; Fax: +86 592 2183047; Tel: +86 592 2184531.

*Stephen P. Cramer. E-mail: spjcramer@ucdavis.edu; Tel: (530) 752-0360.

ORCID

Zhao-Hui Zhou: 0000-0001-7271-7009

Author Contributions

⊥These authors contributed equally.

Notes

The authors declare no competing financial interest.

ACKNOWLEDGMENTS

We thank the National Science Foundation (21773196), the National Science Foundation of Fujian (2016I0101), and NIH GM-65440 (S.P.C.) for their generous financial support. We also thank Ms. La-Jia Yu for help with EPR measurements.

REFERENCES

(1) Sippel, D.; Einsle, O. The structure of vanadium nitrogenase reveals an unusual bridging ligand. *Nat. Chem. Biol.* **2017**, *13*, 956−960.

(2) Spatzal, T.; Aksoyoglu, M.; Zhang, L.; Andrade, S. L. A.; Schleicher, E.; Weber, S.; Rees, D. C.; Einsle, O. Evidence for interstitial carbon in nitrogenase FeMo cofactor. *Science* **2011**, *334*, 940.

(3) Wang, S. Y.; Jin, W. T.; Chen, H. B.; Zhou, Z. H. Comparison of hydroxycarboxylato imidazole molybdenum(iv) complexes and nitrogenase protein structures: indirect evidence for the protonation of homocitrato FeMo-cofactors. *Dalton Trans* **2018**, *47*, 7412−7421.

(4) Lancaster, K. M.; Roemelt, M.; Ettenhuber, P.; Hu, Y.; Ribbe, M. W.; Neese, F.; Bergmann, U.; DeBeer, S. X-ray emission spectroscopy evidences a central carbon in the nitrogenase iron-molybdenum cofactor. *Science* **2011**, *334*, 974−977.

(5) Einsle, O.; Tezcan, F. A.; Andrade, S. L.; Schmid, B.; Yoshida, M.; Howard, J. B.; Rees, D. C. Nitrogenase MoFe-protein at 1.16 Å resolution: a central ligand in the FeMo-cofactor. *Science* **2002**, *297*, 1696−1700.

(6) Kim, J.; Rees, D. C. Structural models for the metal centers in the nitrogenase molybdenum-iron protein. *Science* **1992**, *257*, 1677−1682.

(7) Sippel, D.; Rohde, M.; Netzer, J.; Trncik, C.; Gies, J.; Grunau, K.; Djurdjevic, I.; Decamps, L.; Andrade, S. L. A.; Einsle, O. A bound reaction intermediate sheds light on the mechanism of nitrogenase. *Science* **2018**, *359*, 1484−1489.

(8) Schmid, B.; Ribbe, M. W.; Einsle, O.; Yoshida, M.; Thomas, L. M.; Dean, D. R.; Rees, D. C.; Burgess, B. K. Structure of a cofactor-deficient nitrogenase MoFe protein. *Science* **2002**, *296*, 352−356.

(9) Walters, M. A.; Chapman, S. K.; Orme-Johnson, W. H. The nature of amide ligation to the metal sites of FeMoco (iron-molybdenum cofactor). *Polyhedron* **1986**, *5*, 561−565.

(10) Levchenko, L.; Roschupkina, O.; Sadkov, A.; Marakushev, S.; Mikhailov, G.; Borod'ko, Y. G. Spectroscopic investigation of FeMo-cofactor. Coenzyme A as one of the probable components of an active site of nitrogenase. *Biochem. Biophys. Res. Commun.* **1980**, *96*, 1384−1392.

(11) Robinson, A. E.; Richards, A. J.; Thomson, A. J.; Hawkes, T. R.; Smith, B. E. Low-temperature magnetic-circular-dichroism spectroscopy of the iron-molybdenum cofactor and the complementary cofactor-less MoFe protein of Klebsiella pneumoniae nitrogenase. *Biochem. J.* **1984**, *219*, 495−503.

(12) Stephens, P. J.; McKenna, C. E.; McKenna, M. C.; Nguyen, H. T.; Devlin, F. Circular dichroism and magnetic circular dichroism of reduced molybdenum-iron protein of Azotobacter vinelandii nitrogenase. *Biochemistry* **1981**, *20*, 2857−2864.

(13) Mascharak, P. K.; Smith, M. C.; Armstrong, W. H.; Burgess, B. K.; Holm, R. H. Fluorine-19 chemical shifts as structural probes of metal-sulfur clusters and the cofactor of nitrogenase. *Proc. Natl. Acad. Sci. U. S. A.* **1982**, *79*, 7056−7060.

(14) Conradson, S. D.; Burgess, B. K.; Newton, W. E.; Di Cicco, A.; Filipponi, A.; Wu, Z. Y.; Natoli, C. R.; Hedman, B.; Hodgson, K. O. Selenol binds to iron in nitrogenase iron-molybdenum cofactor: an extended x-ray absorption fine structure study. *Proc. Natl. Acad. Sci. U. S. A.* **1994**, *91*, 1290−1293.

(15) Liu, H. I.; Burgess, B. K.; Natoli, C. R.; Filipponi, A.; Gavini, N.; Hedman, B.; Di Cicco, A.; Hodgson, K. O. EXAFS studies of FeMo-cofactor and MoFe protein: Direct evidence for the long-range Mo-Fe-Fe interaction and cyanide binding to the Mo in FeMo-cofactor. *J. Am. Chem. Soc.* **1994**, *116*, 2418−2423.

(16) Conradson, S. D.; Burgess, B. K.; Newton, W. E.; Mortenson, L. E.; Hodgson, K. O. Structural studies of the molybdenum site in the MoFe protein and its FeMo cofactor by EXAFS. *J. Am. Chem. Soc.* **1987**, *109*, 7507−7515.

(17) Cramer, S. P.; Gillum, W. O.; Hodgson, K. O.; Mortenson, L. E.; Stiefel, E. I.; Chisnell, J. R.; Brill, W. J.; Shah, V. K. The molybdenum site of nitrogenase. 2. A comparative study of molybdenum-iron proteins and the iron-molybdenum cofactor by x-ray absorption spectroscopy. *J. Am. Chem. Soc.* **1978**, *100*, 3814−3819.

(18) Antonio, M. R.; Teo, B. K.; Orme-Johnson, W. H.; Nelson, M. J.; Groh, S. E.; Lindahl, P. A.; Kauzlarich, S. M.; Averill, B. A. Iron EXAFS of the iron-molybdenum cofactor of nitrogenase. *J. Am. Chem. Soc.* **1982**, *104*, 4703−4705.

(19) Arber, J. M.; Flood, A. C.; Garner, C. D.; Gormal, C. A.; Hasnain, S. S.; Smith, B. E. Iron K-edge X-ray absorption spectroscopy of the iron-molybdenum cofactor of nitrogenase from Klebsiella pneumoniae. *Biochem. J.* **1988**, *252*, 421−425.

(20) Rawlings, J.; Shah, V. K.; Chisnell, J. R.; Brill, W. J.; Zimmermann, R.; Münck, E.; Orme-Johnson, W. H. Novel metal cluster in the iron-molybdenum cofactor of nitrogenase. Spectroscopic evidence. *J. Biol. Chem.* **1978**, *253*, 1001−1004.

(21) Newton, W. E.; Gheller, S. F.; Sands, R. H.; Dunham, W. R. Mössbauer spectroscopy applied to the oxidized and semi-reduced states of the iron-molybdenum cofactor of nitrogenase. *Biochem. Biophys. Res. Commun.* **1989**, *162*, 882−891.

(22) Lukoyanov, D.; Pelmenschikov, V.; Maeser, N.; Laryukhin, M.; Yang, T. C.; Noodleman, L.; Dean, D. R.; Case, D. A.; Seefeldt, L. C.; Hoffman, B. M. Testing if the interstitial atom, X, of the nitrogenase molybdenum-iron cofactor is N or C: ENDOR, ESEEM, and DFT studies of the S = 3/2 resting state in multiple environments. *Inorg. Chem.* **2007**, *46*, 11437−11449.

(23) Yang, T. C.; Maeser, N. K.; Laryukhin, M.; Lee, H. I.; Dean, D. R.; Seefeldt, L. C.; Hoffman, B. M. The interstitial atom of the

DOI: 10.1021/acs.inorgchem.8b03108
Inorg. Chem. 2019, 58, 2523−2532

nitrogenase FeMo-cofactor: ENDOR and ESEEM evidence that it is not a nitrogen. *J. Am. Chem. Soc.* **2005**, *127*, 12804−12805.
(24) Delfino, I.; Cerullo, G.; Cannistraro, S.; Manzoni, C.; Polli, D.; Dapper, C.; Newton, W. E.; Guo, Y.; Cramer, S. P. Observation of terahertz vibrations in the nitrogenase FeMo cofactor by femtosecond pump-probe spectroscopy. *Angew. Chem.* **2010**, *122*, 4004−4007.
(25) Xiao, Y.; Fisher, K.; Smith, M. C.; Newton, W. E.; Case, D. A.; George, S. J.; Wang, H.; Sturhahn, W.; Alp, E. E.; Zhao, J.; Yoda, Y.; Cramer, S. P. How Nitrogenase Shakes − Initial Information about P−Cluster and FeMo-cofactor Normal Modes from Nuclear Resonance Vibrational Spectroscopy (NRVS). *J. Am. Chem. Soc.* **2006**, *128*, 7608−7612.
(26) George, S. J.; Igarashi, R. Y.; Xiao, Y.; Hernandez, J. A.; Demuez, M.; Zhao, D.; Yoda, Y.; Ludden, P. W.; Rubio, L. M.; Cramer, S. P. Extended X-ray absorption fine structure and nuclear resonance vibrational spectroscopy reveal that *NifB*-co, a FeMo-co precursor, comprises a 6Fe core with an interstitial light atom. *J. Am. Chem. Soc.* **2008**, *130*, 5673−5680.
(27) Shah, V. K.; Brill, W. J. Isolation of a molybdenum–iron cluster from nitrogenase. *Proc. Natl. Acad. Sci. U. S. A.* **1981**, *78*, 3438−3440.
(28) Lee, H.-I.; Hales, B. J.; Hoffman, B. M. Metal-Ion Valencies of the FeMo Cofactor in CO-Inhibited and Resting State Nitrogenase by 57Fe Q-Band ENDOR. *J. Am. Chem. Soc.* **1997**, *119*, 11395−11400.
(29) Yoo, S. J.; Angove, H. C.; Papaefthymiou, V.; Burgess, B. K.; Münck, E. Mössbauer Study of the MoFe Protein of Nitrogenase from Azotobacter vinelandii Using Selective 57Fe Enrichment of the M-Centers. *J. Am. Chem. Soc.* **2000**, *122*, 4926−4936.
(30) Harris, T. V.; Szilagyi, R. K. Comparative Assessment of the Composition and Charge State of Nitrogenase FeMo-Cofactor. *Inorg. Chem.* **2011**, *50*, 4811−4824.
(31) Bjornsson, R.; Neese, F.; DeBeer, S. Revisiting the Mössbauer Isomer Shifts of the FeMoco Cluster of Nitrogenase and the Cofactor Charge. *Inorg. Chem.* **2017**, *56*, 1470−1477.
(32) Spatzal, T.; Schlesier, J.; Burger, E.-M.; Sippel, D.; Zhang, L.; Andrade, S. L. A.; Rees, D. C.; Einsle, O. Nitrogenase FeMoco investigated by spatially resolved anomalous dispersion refinement. *Nat. Commun.* **2016**, *7*, 10902.
(33) Cao, Z. X.; Jin, X.; Zhou, Z. H.; Zhang, Q. E. Protonation of metal-bound α-hydroxycarboxylate ligand and implication for the role of homocitrate in nitrogenase: computational study of the oxy-bidentate chelate ring opening. *Int. J. Quantum Chem.* **2006**, *106*, 2161−2168.
(34) Chen, C. Y.; Chen, M. L.; Chen, H. B.; Wang, H. X.; Cramer, S. P.; Zhou, Z. H. α-Hydroxy coordination of mononuclear vanadyl citrate, malate and S-citramalate with N-heterocycle ligand, implying a new protonation pathway of iron-vanadium cofactor in nitrogenase. *J. Inorg. Biochem.* **2014**, *141*, 114−120.
(35) Benediktsson, B.; Bjornsson, R. QM/MM study of the nitrogenase MoFe protein resting state: broken-symmetry states, protonation states, and QM region convergence in the FeMoco active site. *Inorg. Chem.* **2017**, *56*, 13417−13429.
(36) Cao, L.; Caldararu, O.; Ryde, U. Protonation states of homocitrate and nearby residues in nitrogenase studied by computational methods and quantum refinement. *J. Phys. Chem. B* **2017**, *121*, 8242−8262.
(37) Siegbahn, P. E. M. A major structural change of the homocitrate ligand of probable importance for the nitrogenase mechanism. *Inorg. Chem.* **2018**, *57*, 1090−1095.
(38) Tsaramyrsi, M.; Kaliva, M.; Salifoglou, A.; Raptopoulou, C. P.; Terzis, A.; Tangoulis, V.; Giapintzakis, J. Vanadium(IV)-citrate complex interconversions in aqueous solutions. A pH-dependent synthetic, structural, spectroscopic, and magnetic study. *Inorg. Chem.* **2001**, *40*, 5772−5779.
(39) Li, X.; Dai, J. W.; Wang, H. X.; Wu, A. A.; Zhou, Z. H. Chiral and achiral vanadyl lactates with vibrational circular dichroism: Toward the chiral metal cluster in nitrogenase. *Inorg. Chim. Acta* **2016**, *453*, 501−506.
(40) Jin, W. T.; Li, X.; Zhou, Z. H. Degradations of novel tetranuclear vanadyl glycollates to dinuclear species. *Polyhedron* **2017**, *122*, 99−104.
(41) Chen, C. Y.; Zhou, Z. H.; Chen, H. B.; Huang, P. Q.; Tsai, K. R.; Chow, Y. L. Formations of mixed-valence oxovanadiumV,IV citrates and homocitrate with N-heterocycle chelated ligand. *Inorg. Chem.* **2008**, *47*, 8714−8720.
(42) Biagioli, M.; Strinna-Erre, L.; Micera, G.; Panzanelli, A.; Zema, M. Molecular structure, characterization and reactivity of dioxo complexes formed by vanadium(V) with α-hydroxycarboxylate ligands. *Inorg. Chim. Acta* **2000**, *310*, 1−9.
(43) Burojevic, S.; Shweky, I.; Bino, A.; Summers, D. A.; Thompson, R. C. Synthesis, structure and magnetic properties of an asymmetric dinuclear oxocitratovanadate(IV) complex. *Inorg. Chim. Acta* **1996**, *251*, 75−79.
(44) Zhou, Z. H.; Wan, H. L.; Hu, S. Z.; Tsai, K. R. Syntheses and structures of the potassium-ammonium dioxocitratovanadate(V) and sodium oxocitratovanadate(IV) dimers. *Inorg. Chim. Acta* **1995**, *237*, 193−197.
(45) Zhou, Z. H.; Wang, J. Z.; Wan, H. L.; Tsai, K. R. Synthesis and structure of $(NH_4)_2[V_2O_4(OCH_2COO)_2]$. *Chem. Res. Chin. Univ.* **1994**, *10*, 102−106.
(46) Wright, D. W.; Humiston, P. A.; Orme-Johnson, W. H.; Davis, W. M. A unique coordination mode for citrate and a transition metal: $K_2[V(O)_2(C_6H_6O_7)]_2\cdot 4H_2O$. *Inorg. Chem.* **1995**, *34*, 4194−4197.
(47) Zhou, Z. H.; Yan, W. B.; Wan, H. L.; Tsai, K. R.; Wang, J. Z.; Hu, S. Z. Metal-hydroxycarboxylate interactions: syntheses and structures of $K_2[VO_2(C_6H_6O_7)]_2\cdot 4H_2O$ and $(NH_4)_2[VO_2(C_6H_6O_7)]_2\cdot 2H_2O$. *J. Chem. Crystallogr.* **1995**, *25*, 807−811.
(48) Tsaramyrsi, M.; Kavousanaki, D.; Raptopoulou, C. P.; Terzis, A.; Salifoglou, A. Systematic synthesis, structural characterization, and reactivity studies of vanadium(V)-citrate anions $[VO_2(C_6H_6O_7)]_2^{2-}$, isolated from aqueous solutions in the presence of different cations. *Inorg. Chim. Acta* **2001**, *320*, 47−59.
(49) Zhou, Z. H.; Zhang, H.; Jiang, Y. Q.; Lin, D. H.; Wan, H. L.; Tsai, K. R. Complexation between vanadium(V) and citrate: spectroscopic and structural characterization of a dinuclear vanadium-(V) complex. *Transition Met. Chem.* **1999**, *24*, 605−609.
(50) Kaliva, M.; Giannadaki, T.; Salifoglou, A.; Raptopoulou, C. P.; Terzis, A. A new dinuclear vanadium(V)-citrate complex from aqueous solutions. synthetic, structural, spectroscopic, and pH-dependent studies in relevance to aqueous vanadium(V)-citrate speciation. *Inorg. Chem.* **2002**, *41*, 3850−3858.
(51) Kaliva, M.; Raptopoulou, C. P.; Terzis, A.; Salifoglou, A. Systematic studies on pH-dependent transformations of dinuclear vanadium(V)-citrate complexes in aqueous solutions. A perspective relevance to aqueous vanadium(V)-citrate speciation. *J. Inorg. Biochem.* **2003**, *93*, 161−173.
(52) Wright, D. W.; Chang, R. T.; Mandal, S. K.; Armstrong, W. H.; Orme-Johnson, W. H. A novel vanadium(V) homocitrate complex: synthesis, structure, and biological relevance of $[K_2(H_2O)_5]$-$[(VO_2)_2(R,S\text{-homocitrate})_2]\cdot H_2O$. *JBIC, J. Biol. Inorg. Chem.* **1996**, *1*, 143−151.
(53) Zhou, Z. H.; Hou, S. Y.; Cao, Z. X.; Wan, H. L.; Ng, S. W. Syntheses, crystal structures and biological relevance of glycolato and S-lactato molybdates. *J. Inorg. Biochem.* **2004**, *98*, 1037−1044.
(54) Zhou, Z. H.; Yan, W. B.; Wan, H. L.; Tsai, K. R. Synthesis and characterization of homochiral polymeric S-malato molybdate(VI): toward the potentially stereospecific formation and absolute configuration of iron-molybdenum cofactor in nitrogenase. *J. Inorg. Biochem.* **2002**, *90*, 137−143.
(55) Knobler, C. B.; Wilson, A. J.; Hider, R. N.; Jensen, I. W.; Penfold, B. R.; Robinson, W. T.; Wilkins, C. J. Molybdenum(VI) complexes with malic acid: their inter-relationships, and the crystal structure of dicaesium bis[(S)-malato(2-)]-cis-dioxomolybdate(VI)-water (1/1). *J. Chem. Soc., Dalton Trans.* **1983**, *7*, 1299−1303.
(56) Zhou, Z. H.; Wan, H. L.; Tsai, K. R. Syntheses and spectroscopic and structural characterization of molybdenum(VI)

DOI: 10.1021/acs.inorgchem.8b03108
Inorg. Chem. 2019, 58, 2523−2532

citrato monomeric raceme and dimer, $K_4[MoO_3(cit)]\cdot 2H_2O$ and $K_4[(MoO_2)_2O(Hcit)_2]\cdot 4H_2O$. *Inorg. Chem.* **2000**, *39*, 59−64.
(57) Zhang, R. H.; Zhou, X. W.; Guo, Y. C.; Chen, M. L.; Cao, Z. X.; Chow, Y. L.; Zhou, Z. H. Crystalline and solution chemistry of tetrameric and dimeric molybdenum(VI) citrato complexes. *Inorg. Chim. Acta* **2013**, *406*, 27−36.
(58) Zhou, Z. H.; Chen, C. Y.; Cao, Z. X.; Tsai, K. R.; Chow, Y. L. N-heterocycle chelated oxomolybdenum(VI and V) complexes with bidentate citrate. *Dalton Trans* **2008**, *252*, 2475−2479.
(59) Zhou, Z. H.; Deng, Y. F.; Cao, Z. X.; Zhang, R. H.; Chow, Y. L. Dimeric dioxomolybdenum(VI) and oxomolybdenum(V) complexes with citrate at very low pH and neutral conditions. *Inorg. Chem.* **2005**, *44*, 6912−6914.
(60) Zhou, Z. H.; Hou, S. Y.; Cao, Z. X.; Tsai, K. R.; Chow, Y. L. Syntheses, spectroscopies and structures of molybdenum(VI) complexes with homocitrate. *Inorg. Chem.* **2006**, *45*, 8447−8451.
(61) Zhou, Z. H.; Wang, H. x.; Yu, P.; Olmstead, M. M.; Cramer, S. P. Structure and spectroscopy of a bidentate bis-homocitrate dioxomolybdenum(VI) complex: Insights relevant to the structure and properties of the FeMo-cofactor in nitrogenase. *J. Inorg. Biochem.* **2013**, *118*, 100−106.
(62) Li, D. M.; Xing, Y. H.; Li, Z. C.; Xu, J. Q.; Song, W. B.; Wang, T. G.; Yang, G. D.; Hu, N. H.; Jia, H. Q.; Zhang, H. M. Synthesis and characterization of binuclear molybdenum−polycarboxylate complexes with sulfur bridges. *J. Inorg. Biochem.* **2005**, *99*, 1602−1610.
(63) Xing, Y. H.; Xu, J. Q.; Sun, H. R.; Li, D. M.; Xing, Y.; Lin, Y. H.; Jia, H. Q. A new dinuclear molybdenum(V)-sulfur complex containing citrate ligand: Synthesis and characterization of $K_{2.5}Na_2NH_4[Mo_2O_2S_2(cit)_2]\cdot 5H_2O$. *Eur. J. Solid State Inorg. Chem.* **1998**, *35*, 745−756.
(64) Huang, J. L.; Zhou, K. J.; Lu, J. The crystal and molecular structure of dipotassium tris(hydroxyacetato)vanadyl(IV) monohydrate. *Sci. Sin., Ser. B* **1986**, *29*, 1−7.
(65) Guilherme, L. R.; Massabni, A. C.; Cuin, A.; Oliveira, L. A. A.; Castellano, E. E.; Heinrich, T. A.; Costa-Neto, C. M. Synthesis, characterization, crystal structure, and biological studies of vanadium complexes with glycolic acid. *J. Coord. Chem.* **2009**, *62*, 1561−1571.
(66) Jodaian, V.; Mirzaei, M.; Arca, M.; Carla Aragoni, M.; Lippolis, V.; Tavakoli, E.; Langeroodi, N. S. First example of a 1:1 vanadium(IV)-citrate complex featuring the 2,2'-bipyridine co-ligand: Synthesis, X-ray crystal structure and DFT calculations. *Inorg. Chim. Acta* **2013**, *400*, 107−114.
(67) Sokolov, M. N.; Adonin, S. A.; Virovets, A. V.; Abramov, P. A.; Vicent, C.; Llusar, R.; Fedin, V. P. Complexes of $M_3S_4^{4+}$ (M = Mo, W) with chiral alpha-hydroxy and aminoacids: Synthesis, structure and solution studies. *Inorg. Chim. Acta* **2013**, *395*, 11−18.
(68) Takuma, M.; Ohki, Y.; Tatsumi, K. Molybdenum carbonyl complexes with citrate and its relevant carboxylates. *Organometallics* **2005**, *24*, 1344−1347.
(69) Fay, A. W.; Lee, C. C.; Wiig, J. A.; Hu, Y.; Ribbe, M. W. In *Nitrogen Fixation: Methods and Protocols*; Ribbe, M. W., Ed.; Humana Press: Totowa, NJ, 2011; pp 239−248.
(70) Shah, V. K.; Brill, W. J. Isolation of an iron-molybdenum cofactor from nitrogenase. *Proc. Natl. Acad. Sci. U. S. A.* **1977**, *74*, 3249−3253.
(71) Brese, N. E.; O'keeffe, M. Bond-valence parameters for solids. *Acta Crystallogr., Sect. B: Struct. Sci.* **1991**, *B47*, 192−197.
(72) Brown, I. D. *The chemical bond in inorganic chemistry: the bond valence model*. Oxford University Press on Demand: 2002; Vol. *12*.
(73) Rees, J. A.; Bjornsson, R.; Kowalska, J. K.; Lima, F. A.; Schlesier, J.; Sippel, D.; Weyhermueller, T.; Einsle, O.; Kovacs, J. A.; De Beer, S. Comparative electronic structures of nitrogenase FeMoco and FeVco. *Dalton Trans* **2017**, *46*, 2445−2455.
(74) True, A. E.; McLean, P.; Nelson, M. J.; Orme-Johnson, W.; Hoffman, B. M. Comparison of wild-type and nifV mutant molybdenum-iron proteins of nitrogenase from Klebsiella pneumoniae by ENDOR spectroscopy. *J. Am. Chem. Soc.* **1990**, *112*, 651−657.
(75) Bjornsson, R.; Lima, F. A.; Spatzal, T.; Weyhermuller, T.; Glatzel, P.; Bill, E.; Einsle, O.; Neese, F.; DeBeer, S. Identification of a spin-coupled Mo(III) in the nitrogenase iron-molybdenum cofactor. *Chem. Sci.* **2014**, *5*, 3096−3103.
(76) Bjornsson, R.; Neese, F.; Schrock, R. R.; Einsle, O.; DeBeer, S. The discovery of Mo(III) in FeMoco: reuniting enzyme and model chemistry. *JBIC, J. Biol. Inorg. Chem.* **2015**, *20*, 447−460.
(77) Otieno, T.; Bond, M. R.; Mokry, L. M.; Walter, R. B.; Carrano, C. J. Plasmid DNA cleavage by oxo-bridged vanadium(III) dimers without added co-oxidants or reductants. *Chem. Commun.* **1996**, *1*, 37−38.
(78) Brand, S. G.; Edelstein, N.; Hawkins, C. J.; Shalimoff, G.; Snow, M. R.; Tiekink, E. R. T. An oxo-bridged binuclear vanadium(III) 2,2'-bipyridine complex and its vanadium(IV) and vanadium(V) oxidation products. *Inorg. Chem.* **1990**, *29*, 434−438.
(79) Deacon, G. B.; Phillips, R. J. Relationships between the carbon-oxygen stretching frequencies of carboxylato complexes and the type of carboxylate coordination. *Coord. Chem. Rev.* **1980**, *33*, 227−250.
(80) Rehder, D.; Pessoa, J. C.; Geraldes, C. F. G. C.; Castro, M. M. C. A.; Kabanos, T.; Kiss, T.; Meier, B.; Micera, G.; Pettersson, L.; Rangel, M.; Salifoglou, A.; Turel, I.; Wang, D. In vitro study of the insulin-mimetic behaviour of vanadium(IV, V) coordination compounds. *JBIC, J. Biol. Inorg. Chem.* **2002**, *7*, 384−396.
(81) Velayutham, M.; Varghese, B.; Subramanian, S. Magneto-structural correlation studies of a ferromagnetically coupled dinuclear vanadium(IV) complex. Single-crystal EPR study. *Inorg. Chem.* **1998**, *37*, 1336−1340.
(82) Silverstein, R. M.; Bassler, G. C.; Morrill, T. *Spectrometric Identification of Organic Compounds*, 5th ed.; John Wiley & Sons, Inc.: Hoboken, NJ, 1991; pp 110−115.
(83) Strandberg, G. W.; Wilson, P. W. Formation of the nitrogen-fixing enzyme system in Azotobacter vinelandii. *Can. J. Microbiol.* **1968**, *14*, 25−31.
(84) Kim, C. H.; Newton, W. E.; Dean, D. R. Role of the MoFe protein. α-subunit histidine-195 residue in FeMo-cofactor binding and nitrogenase catalysis. *Biochemistry* **1995**, *34*, 2798−2808.
(85) Paustian, T. D.; Shah, V. K.; Roberts, G. P. Apodinitrogenase: purification, association with a 20-kilodalton protein, and activation by the iron-molybdenum cofactor in the absence of dinitrogenase reductase. *Biochemistry* **1990**, *29*, 3515−3522.
(86) Sheldrick, G. M. A short history of SHELX. *Acta Crystallogr., Sect. A: Found. Crystallogr.* **2008**, *A64*, 112−122.
(87) Dolomanov, O. V.; Bourhis, L. J.; Gildea, R. J.; Howard, J. A. K.; Puschmann, H. OLEX2: a complete structure solution, refinement and analysis program. *J. Appl. Crystallogr.* **2009**, *42*, 339−341.
(88) Sheldrick, G. M. Crystal structure refinement with SHELXL. *Acta Crystallogr., Sect. C: Struct. Chem.* **2015**, *C71*, 3−8.
(89) Frisch, M. J.; G. W. T, Schlegel, H. B.; Scuseria, G. E.; Robb, M. A.; Cheeseman, J. R.; Scalmani, G.; Barone, V.; Mennucci, B.; Petersson, G. A.; Nakatsuji, H.; Caricato, M.; Li, X.; Hratchian, H. P.; Izmaylov, A. F.; Bloino, J.; Zheng, G.; Sonnenberg, J. L.; Hada, M.; Ehara, M.; Toyota, K.; Fukuda, R.; Hasegawa, J.; Ishida, M.; Nakajima, T.; Honda, Y.; Kitao, O.; Nakai, H.; Vreven, T.; Montgomery, J. A., Jr., Peralta, J. E.; Ogliaro, F.; Bearpark, M.; Heyd, J. J.; Brothers, E.; Kudin, K. N.; Staroverov, V. N.; Kobayashi, R.; Normand, J.; Raghavachari, K.; Rendell, A.; Burant, J. C.; Iyengar, S. S.; Tomasi, J.; Cossi, M.; Rega, N.; Millam, J. M.; Klene, M.; Knox, J. E.; Cross, J. B.; Bakken, V.; Adamo, C.; Jaramillo, J.; Gomperts, R.; Stratmann, R. E.; Yazyev, O.; Austin, A. J.; Cammi, R.; Pomelli, C.; Ochterski, J. W.; Martin, R. L.; Morokuma, K.; Zakrzewski, V. G.; Voth, G. A.; Salvador, P.; Dannenberg, J. J.; Dapprich, S.; Daniels, A. D.; Farkas, Ö., Foresman, J. B.; Ortiz, J. V.; Cioslowski, J.; Fox, D. J. *Gaussian 09*; Gaussian, Inc.: Wallingford, CT, 2009.

DOI: 10.1021/acs.inorgchem.8b03108
Inorg. Chem. 2019, 58, 2523−2532